



CrossMark  
click for updates

Cite this: *RSC Adv.*, 2014, 4, 33658

Received 3rd June 2014  
Accepted 16th July 2014

DOI: 10.1039/c4ra05255b

www.rsc.org/advances

# Facile preparation of novel Au–polydopamine nanoparticles modified by 4-mercaptophenylboronic acid for use in a glucose sensor†

Guohua Jiang,<sup>\*abc</sup> Tengteng Jiang,<sup>ab</sup> Yuan Wang,<sup>d</sup> Xiangxiang Du,<sup>ab</sup> Zhen Wei<sup>ab</sup> and Huijie Zhou<sup>d</sup>

Au nanoparticles were attached to the surface of polydopamine (PDA) microspheres by an *in situ* reduction reaction between PDA and HAuCl<sub>4</sub>. 4-Mercaptophenyl boronic acid (MPBA) was then modified to form Au–PDA composite particles *via* a strong Au–S interaction. The resultant MPBA–Au–PDA particles were used in a non-enzyme amperometric glucose sensor.

## Introduction

Glucose is a carbohydrate and is the most important simple sugar in human metabolism. The normal concentration of glucose in blood is about 0.1%, but this is much higher in patients with diabetes. From a clinical perspective, there is a need for high-sensitivity, low-cost methods with good reproducibility for the rapid and accurate determination of glucose.<sup>1,2</sup> Much work has been carried out to develop methods to monitor glucose concentrations in the human body. Of these, enzyme-free electrochemical sensors have become highly desirable as these avoid the use and sophisticated manufacture of glucose oxidase (GODx) and are aimed at the direct oxidation of glucose in blood samples.<sup>3</sup> However, poor measurement stability as a result of surface poisoning from adsorbed intermediate products and the effect of coexisting electroactive species are still serious problems in the application of electrochemical sensor materials.

Recent advances in nanomaterial science and nanotechnology have provided new opportunities for the development of enzyme-free glucose sensors. Nanomaterials of noble metals

(*e.g.* Pt,<sup>4</sup> Pd<sup>5</sup> and Au<sup>6</sup>), non-noble metals (*e.g.* Cu<sup>7</sup> and Ni<sup>8</sup>), metal oxides (*e.g.* Co<sub>3</sub>O<sub>4</sub>,<sup>9</sup> Mn<sub>x</sub>O<sub>y</sub> (ref. 10) and Fe<sub>x</sub>O<sub>y</sub> (ref. 11)) and bimetallic composites<sup>12</sup> have been widely used to produce novel electrochemical enzyme-free glucose sensors. In most instances these sensors use carbon materials as supporting materials to enhance the electron transfer ability and to increase the surface area of the metal nanomaterials. For example, Pt nanoflowers (PtNF) are synthesized on a single-walled carbon nanotubes (SWCNT) film using electrodeposition. The as-prepared PtNF film has an excellent catalytic ability towards the amperometric detection of glucose at neutral pH.<sup>13</sup> Chen *et al.*<sup>14</sup> have prepared PtNF and graphene oxide composites that show a wide linear response for glucose from 2 μM to 20.3 mM.

Dopamine (3,4-dihydroxyphenylethylamine) (DA), an important hormone and neurotransmitter, has a significant physiological role in mammals as a chemical messenger. In the presence of dissolved O<sub>2</sub> and under alkaline conditions, an aqueous solution of DA will spontaneously oxidize to polydopamine (PDA), yielding a melanin-like polymer that can be deposited on both organic and inorganic surfaces.<sup>15</sup> Furthermore, PDA contains catechol functional groups, which makes it an efficient matrix for loading thiol- or amine-containing molecules through the formation of thiol- and amine-catechol adducts. This PDA functionalization therefore provides an extremely versatile platform, not only for the immobilization of biological molecules, but also for the possible *in situ* deposition of metallic nanoparticles (NPs).<sup>16,17</sup> The *in situ* deposition of high-content metallic NPs on the PDA not only provides a simple and controllable method for the preparation of nanoprobe, but also amplifies the signal response of each immune-recognition event.

In the work reported here, PDA microspheres were first prepared by the polymerization of DA in the presence of F108 as a template surfactant under alkaline conditions.<sup>18</sup> As a result of the abundant functional groups (–OH, –NH<sub>2</sub>) on the surface of the PDA spheres, they showed an extraordinarily versatile active nature and had the ability to reduce AuCl<sub>4</sub><sup>–</sup> ions to Au NPs.<sup>19</sup> The Au NPs were attached to the surface of the PDA microspheres by an *in situ* reduction reaction between PDA and

<sup>a</sup>Department of Materials Engineering, Zhejiang Sci-Tech University, Hangzhou 310018, P. R. China. E-mail: ghjiang\_cn@zstu.edu.cn; Tel: +86 571 86843527

<sup>b</sup>National Engineering Laboratory for Textile Fiber Materials and Processing Technology (Zhejiang), Hangzhou 310018, P. R. China

<sup>c</sup>Key Laboratory of Advanced Textile Materials and Manufacturing Technology (ATMT), Ministry of Education, Hangzhou 310018, P. R. China

<sup>d</sup>Qixin Honours School, Zhejiang Sci-Tech University, Hangzhou 310018, P. R. China

† Electronic supplementary information (ESI) available: Details of materials, synthesis of PDA microspheres, preparation of Au–PDA microspheres, preparation of MPBA–Au–PDA nanocomposites, characterization, calculation of the size of Au NPs and calculation of LOD. See DOI: 10.1039/c4ra05255b

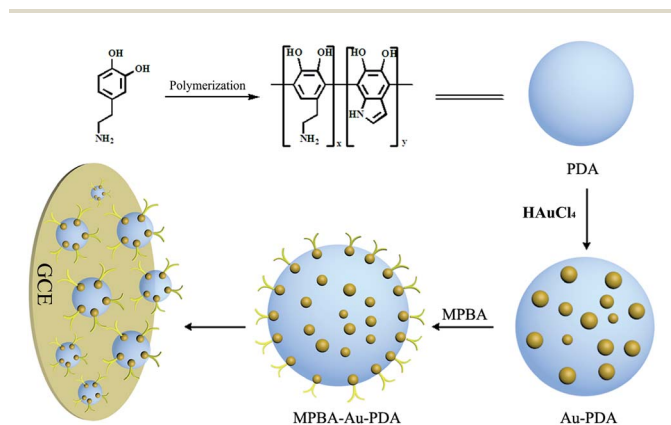
$\text{HAuCl}_4$  to form Au-PDA composite particles. Au-PDA composite particles modified by 4-mercaptophenyl boronic acid (MPBA-Au-PDA) were then prepared by *via* a strong Au-S interaction. The resultant MPBA-Au-PDA particles were used to prepare a non-enzyme amperometric glucose sensor, as shown in Scheme 1 (details of the preparation are given in the ESI†).

## Results and discussion

The black PDA solution is formed after polymerization. The morphology and size of the PDA particles obtained here (pH 8.0) were analyzed by scanning electron microscopy (SEM) and transmission electron microscopy (TEM) (Fig. S1 in ESI†). Spherical particles with sizes of about 120 nm (Fig. 1A and B) were seen, which is consistent with the dynamic light scattering result at 123.4 nm (Fig. S2 in ESI†). As a result of the reducing ability and metal-binding affinity of the catechol groups of PDA,<sup>20</sup>  $\text{HAuCl}_4$  was reduced to Au NPs; this gave the reactive solution a golden color and the Au NPs were immobilized on the surface of PDA (Fig. S3 in ESI†). As shown in Fig. 1C, Au NPs <10

nm in size were seen. A typical HRTEM image (inset in Fig. 1C) with clear lattice fringes with a spacing of about 0.25 nm showed that the growth of Au NPs occurred preferentially on the (111) plane.<sup>21</sup> The electron diffraction pattern of Au-PDA shows non-continuous, but spotty, diffraction rings (Fig. 1D), indicating the presence of some grains of the hydride phases during the formation process of the Au NPs.

The XRD patterns of the as-synthesized PDA and Au-PDA are shown in Fig. 2A. As a result of the amorphous crystallinity of the PDA, an obvious diffraction peak at  $20^\circ$  can be observed for PDA.<sup>22</sup> The crystal structure of the as-prepared Au-PDA hybrid was also confirmed by XRD characterization (Fig. 2A). Apart from the diffraction peak of PDA, major diffraction peaks at Bragg angles of  $38.4^\circ$ ,  $44.4^\circ$ ,  $64.8^\circ$ , and  $77.8^\circ$  and  $81.9^\circ$  were observed, which can be indexed to the (111), (200), (220) and (311) reflections of the face-centered cubic (fcc) phase of metallic gold (JCPDS, card no. 04-0784), respectively, showing the crystalline nature of the particles.<sup>23</sup> The results also indicate that the Au NPs were well dispersed on the PDA particles. The average size of the Au NPs is 9.63 nm as calculated by the Scherrer formula (see calculation in ESI†), which is in good agreement with the results from the TEM image. By using the specific strong Au-S interaction, MPBA molecules can be introduced onto the surface of the Au NPs to form an MPBA-Au-PDA hybrid; the linkage was confirmed by infrared spectroscopy (Fig. 2B). PDA had a broad peak around  $3400\text{ cm}^{-1}$  ascribed to aromatic  $-\text{NH}_x$  and  $-\text{OH}$  stretching vibrations. It also displayed peaks at  $2920\text{ cm}^{-1}$  and  $2850\text{ cm}^{-1}$  (C-H stretching vibrations),  $1600\text{ cm}^{-1}$  (the overlap of C=C resonance vibrations in the aromatic ring) and  $1510\text{ cm}^{-1}$  (N-H scissoring vibrations).<sup>24</sup> Interestingly, after modification by Au and MPBA, the peaks at  $3400\text{ cm}^{-1}$  and  $1601\text{ cm}^{-1}$  became narrower with reduced peak intensity due to the oxidation of  $-\text{NH}_x$  during the formation of the Au NPs. Two new strong peaks at  $1390$  and  $1350\text{ cm}^{-1}$  ascribed to the B-O stretching vibrations of boronic acid in MPBA were also observed.<sup>25</sup> EDS was used to further verify the presence of Au and MPBA in the Au-PDA and MPBA-Au-PDA systems. It was found that the C, O and Au atoms were in the Au-PDA. After modification by MPBA, a new S atomic signal from the thiol group of MPBA was observed (Fig. 2C).



Scheme 1 Schematic illustration of the preparation of the MPBA-Au-PDA modified glassy carbon electrode (GCE).

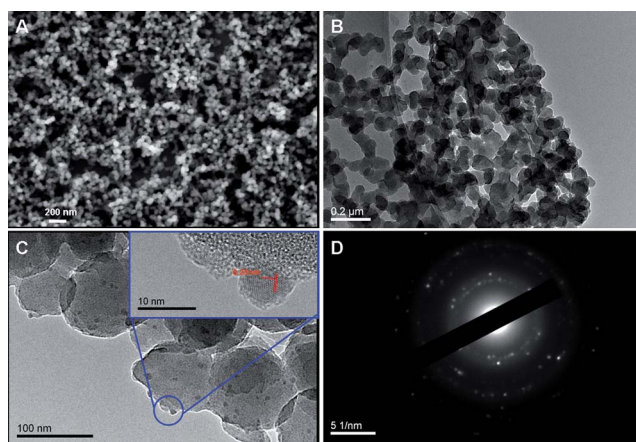


Fig. 1 (A) SEM and (B) TEM images of PDA particles. (C) TEM image of MPBA-Au-PDA particles; inset shows an HRTEM image of the Au NPs. (D) Electron diffraction pattern of a nano-sized region containing Au NPs.

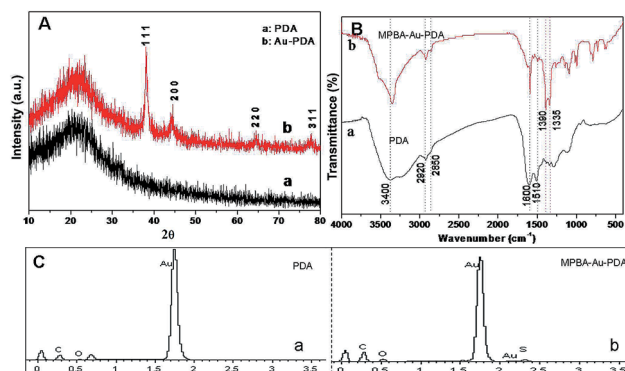


Fig. 2 (A) XRD patterns of PDA and Au-PDA. (B) FTIR spectra of PDA and MPBA-Au-PDA. (C) EDS spectra of Au-PDA and MPBA-Au-PDA.

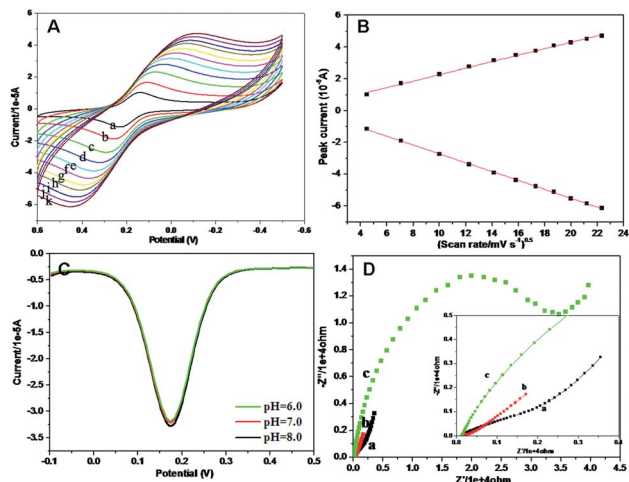


Fig. 3 (A) Cyclic voltammograms curves of MBPA–Au–PDA in  $0.1 \text{ mol L}^{-1}$  PBS at different scan rates (a: 20; b: 50; c: 100; d: 150; e: 200; f: 250; g: 300; h: 350; i: 400; j: 450; and k:  $500 \text{ mV s}^{-1}$ ). (B) Relation between peak current and the square root of the scan rate. (C) DPVs of MPBA–Au–PDA in  $0.1 \text{ mol L}^{-1}$  PBS at various pH values (green line, pH 6; red line, pH 7; and black line, pH 8) and concentration of D-glucose controlled at  $6.0 \text{ mmol L}^{-1}$ . (D) Nyquist plots of (a) bare glassy carbon electrode, (b) Au–PDA electrode and (c) MPBA–Au–PDA electrode in  $0.1 \text{ mol L}^{-1}$  KCl and  $5.0 \text{ mmol L}^{-1} \text{K}_3[\text{Fe}(\text{CN})_6]$ .

Fig. 3A shows cyclic voltammograms in  $0.1 \text{ mol L}^{-1}$  PBS in the potential range  $-0.6$  to  $0.6 \text{ V}$  with a scan rate from  $20$  to  $500 \text{ mV s}^{-1}$  at the MBPA–Au–PDA electrode. As expected, the voltammograms had well-defined redox peaks and the peak currents increased gradually with increasing scan rates. Fig. 3B shows the relationship between the peak current and the square root of the scan rate obtained from the experimental data in Fig. 3A. The anodic and cathodic peak currents both show a linear dependence on the square root of the scan rate. The linear regression equations were as follows:  $I_{pc} = 0.2029V^{1/2} + 0.24306$ ,  $R = 0.99745$ ;  $I_{pa} = -0.27848V^{1/2} + 0.06087$ ,  $R = 0.99962$ . This deviation from a linear relationship suggests that the redox reaction of MBPA–Au–PDA is a surface-controlled process, not a diffusion-controlled process.<sup>26</sup> The pH of the electrolyte can affect the stability of the MBPA–Au–PDA electrode, as reported previously.<sup>20</sup> In this work, the electrochemical response of MBPA–Au–PDA was examined in  $0.1 \text{ mol L}^{-1}$  PBS solutions at various pH values. As shown in Fig. 3C, the redox peak potential barely changed with increasing pH, indicating that no proton is involved in the electrochemical reaction of MBPA. Interestingly, although the peak current had a tendency to decrease, it changed only slightly, suggesting that the working electrode could be used over a wide pH range. It is probable that the Au NPs and PDA increased the stability of MBPA. Boronic acid usually has a high  $pK_a$  value of about  $8.2$ ,<sup>27,28</sup> whereas the boronate ester has a higher acidity ( $pK_a$   $6.0$ ). Therefore a pH value close to the physiological pH of  $7.0$  was used in these experiments. Electrochemical impedance spectroscopy (EIS) was used for further characterization of the modified electrode. EIS is also a highly effective method for probing the features of a surface-modified electrode. In EIS, the semicircle diameter of

the impedance is equal to the electron transfer resistance ( $R_{et}$ ), which controls the electron transfer kinetics of the redox probe at the electrode surface.<sup>3</sup> Fig. 3D shows Nyquist plots of a bare glassy carbon electrode and Au–PDA- and MPBA–Au–PDA-modified electrodes in  $0.1 \text{ mol L}^{-1}$  KCl and  $5.0 \text{ mmol L}^{-1} \text{K}_3[\text{Fe}(\text{CN})_6]$ . The bare GCE (curve a) shows a small semicircle with an  $R_{et}$  of about  $300 \Omega$  at high frequencies. After the bare electrode had been modified with the Au–PDA hybrid, the electrode showed a much lower resistance for the redox probe (curve b), implying that the Au–PDA hybrid was an excellent electrical conducting material and accelerated the electron transfer. After the electrodes had been modified by MPBA–Au–PDA, the Nyquist plots of the MPBA–Au–PDA-modified electrode consisted of a semicircle at high frequency and a straight line at low frequency. The  $R_{et}$  value increased significantly to about  $2000 \Omega$  (curve c), which indicated the formation of a complex layer embracing the electron transfer. The middle frequency semicircle is attributed to charge transfer and the low frequency line to ion diffusion. These results are consistent with those obtained by cyclic voltammetry.

With the addition of glucose, MPBA reacts with the 1,2-diol of D-glucose to form a stable five-membered cyclic boronate ester. A non-enzyme based amperometric glucose sensor was therefore fabricated with MPBA–Au–PDA as the electrochemical indicator. The decreased peak current should be proportional to the concentration of D-glucose (Fig. 4A). Fig. 4B shows the DPV responses of the MPBA–Au–PDA-modified electrodes to different concentrations of D-glucose solution ( $0.1 \text{ M}$  PBS, pH  $7.0$ ) in range  $0$ – $18 \text{ mmol L}^{-1}$ . The peak current decreased with increasing concentration of D-glucose from  $0$  to  $18 \text{ mmol L}^{-1}$ . The regression equation is:  $Y = -4.453 \times 10^{-5} + 1.952 \times 10^{-6} C$  ( $\text{mmol L}^{-1}$ ),  $R = 0.9953$ , as shown in Fig. 4C. A detection limit of

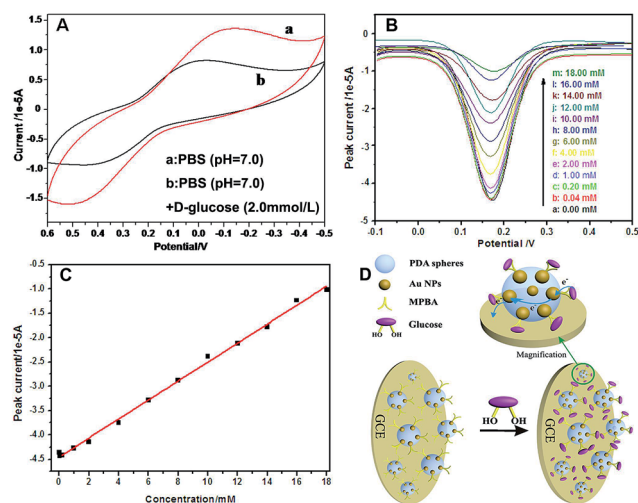


Fig. 4 (A) Cyclic voltammograms curves of MPBA–Au–PDA modified electrodes at a scan rate of  $50 \text{ mV s}^{-1}$  in (a)  $0.1 \text{ mol L}^{-1}$  PBS (pH  $7.0$ ) and (b) with a concentration of D-glucose of  $2 \text{ mmol L}^{-1}$ . (B) DPVs of MPBA–Au–PDA electrode in  $0.1 \text{ mol L}^{-1}$  PBS at pH  $7$  and with the concentration of D-glucose increasing from  $0$  to  $18 \text{ mmol L}^{-1}$  (a:  $0.00$ ; b:  $0.04$ ; c:  $0.20$ ; d:  $1.00$ ; e:  $2.00$ ; f:  $4.00$ ; g:  $6.00$ ; h:  $8.00$ ; i:  $10.00$ ; j:  $12.00$ ; k:  $14.00$ ; l:  $16.00$ ; and m:  $18.00 \text{ mM}$ ). (C) Linear relationship between the peak current and the concentration of D-glucose. (D) Mechanism of binding between MPBA and D-glucose.

$5.0 \times 10^{-8}$  M was estimated using the  $3\sigma$  method (see calculation in ESI†). Compared with other glucose sensors,<sup>29–34</sup> this sensor has a wide linear range, high sensitivity, low detection limit and excellent reproducibility. For example, the C<sub>60</sub>-TOAB<sup>+</sup> composite for glucose detection<sup>34</sup> has a linear response range from 500 nM to 13 mM and a detection limit of  $1.67 \times 10^{-7}$  M. Although the proposed sensor has a linear range that is not in the range of blood sugar levels in humans, it can be used in real sample analysis if the sample is simply diluted. As shown in Fig. 4D, the binding between MPBA and D-glucose obstructed the diffusion of ions across the composite matrix as well as the electron transfer, which was reflected by the decreased peak current.

## Conclusions

In summary, novel MPBA-modified Au NPs were deposited *in situ* on PDA microspheres for use in an ultrasensitive non-enzymatic electrochemical immunoassay for glucose. This *in situ* deposition method provides a simple and controllable way to prepare a novel glucose sensor. The proposed immobilization strategy provides a useful platform for an electrochemical immunoassay for a wide range of glucose concentrations and could be readily extended to the onsite clinical monitoring of blood glucose levels of patients with diabetes. This approach is simple, inexpensive, quick and “green”. Based on the good chemical stability and excellent hydrophilic and biocompatible properties of PDA, the design and synthesis of multi-functional PDA-based bio-nanocomposites with interesting properties has been shown to be an efficient approach for the construction of high-performance biosensors.

## Acknowledgements

This work was financially supported by the National Natural Science Foundation of China (51373155), “521 Talents Training Plan” in Zhejiang Sci-Tech University and the National Training Programs of Innovation and Entrepreneurship for Undergraduates (H. Zhou).

## Notes and references

- G. Jiang, T. Jiang, X. Li, Z. Wei, X. Du and X. Wang, *Mater. Res. Express*, 2014, **1**, 025708.
- T. Jiang, G. Jiang, X. Wang, Y. Dong, Z. Wei, X. Li and B. Tang, *Des. Monomers Polym.*, 2014, **17**, 576–581.
- Z. Wang, K. Shang, J. Dong, Z. Cheng and S. Ai, *Microchim. Acta*, 2012, **179**, 227–234.
- L. Xu, Y. Zhu, L. Tang, X. Yang and C. Li, *Electroanalysis*, 2007, **19**, 717–722.
- C. Yang, X. Zhang, G. Lan, L. Chen, M. Chen, Y. Zeng and J. Jiang, *Chin. Chem. Lett.*, 2014, **25**, 496–500.
- Y. Wu and S. Hu, *Bioelectrochemistry*, 2007, **70**, 335–341.
- X. Kang, Z. Mai, X. Zou, P. Cai and J. Mo, *Chin. Chem. Lett.*, 2007, **18**, 189–191.
- M. Yousef Elahi, H. Heli, S. Z. Bathaie and M. F. Mousavi, *J. Solid State Electrochem.*, 2007, **11**, 273–282.
- C. Hou, Q. Xu, L. Yin and X. Hu, *Analyst*, 2012, **137**, 5803–5808.
- J. Yu and S. Hu, *Electrochim. Acta*, 2010, **55**, 3471–3476.
- S. Masoomi-Godarzi, A. A. Khodadadi, M. Vesali-Naseh and Y. Mortazavi, *J. Electrochem. Soc.*, 2014, **161**, 19–25.
- X. Cao, N. Wang, S. Jia and Y. Shao, *Anal. Chem.*, 2013, **85**, 5040–5046.
- L. Su, W. Jia, L. Zhang, C. Beacham, H. Zhang and Y. Lei, *J. Phys. Chem. C*, 2010, **114**, 18121–18125.
- G. Wu, X. Song, Y. Wu, X. Chen, F. Luo and X. Chen, *Talanta*, 2013, **105**, 379–385.
- F. Li, L. Yang, C. Zhao, Z. Du, F. Luo and X. Chen, *Anal. Methods*, 2011, **3**, 1601–1606.
- K. Jia, M. Khaywah, Y. Li, J. Bijeon, P. Adam, R. D eturche, B. Guelorget, M. Fran ois, G. Louarn and R. Ionescu, *ACS Appl. Mater. Interfaces*, 2014, **6**, 219–227.
- M. Sureshkumar, P.-N. Lee and C.-K. Lee, *J. Mater. Chem.*, 2011, **21**, 12316–12320.
- J. Yan, L. Yang, M.-F. Lin, J. Ma, X. Lu and P. Lee, *Small*, 2013, **9**, 596–603.
- Z. Ma, X. Jia, J. Hu, F. Zhou and B. Dai, *RSC Adv.*, 2014, **4**, 1853–1856.
- J. Li, Z. Wang, P. Li, N. Zong and F. Li, *Sens. Actuators, B*, 2012, **161**, 832–837.
- Y. Miao, H. Ascolani, G. Zampieri, D. Woodruff, C. Satterley, J. Robert and V. Dhanak, *J. Phys. Chem. C*, 2007, **111**, 10904–10914.
- M. Zhang, X. He, L. Chen and Y. Zhang, *J. Mater. Chem.*, 2010, **20**, 10696–10704.
- R. Liang, X. Meng, C. Liu and J. Qiu, *Electrophoresis*, 2011, **32**, 3331–3340.
- R. Luo, L. Tang, S. Zhong, Z. Yang, J. Wang, Y. Weng, Q. Tu, C. Jiang and N. Huang, *ACS Appl. Mater. Interfaces*, 2013, **5**, 1704–1714.
- A. Kawamoto, L. Pardini, M. Diniz, V. Lourenco and M. Takahashi, *J. Aerosp. Technol. Manage.*, 2010, **2**, 169–182.
- Y. Zhu and C. Wang, *J. Phys. Chem. C*, 2011, **115**, 823–832.
- Z. Xu, K. Uddin, T. Kamra, J. Schnadt and L. Ye, *ACS Appl. Mater. Interfaces*, 2014, **6**, 1406–1414.
- B. Kumar, K. Salikolimi and M. Eswaramoorthy, *Langmuir*, 2014, **30**, 4540–4544.
- X. Xiao, M. Wang, H. Li, Y. Pan and P. Si, *Talanta*, 2014, **125**, 366–371.
- T. Alizadeh and S. Mirzaghilipour, *Sens. Actuators, B*, 2014, **198**, 438–447.
- E. Sharifi, A. Salimi, E. Shams, A. Noorbakhsh and M. K. Amini, *Biosens. Bioelectron.*, 2014, **56**, 313–319.
- Y. Li, X. Niu, J. Tang, M. Lan and H. Zhao, *Electrochim. Acta*, 2014, **130**, 1–8.
- K. Dhara, J. Stanley, T. Ramachandran, B. G. Nair and S. Babu, *Sens. Actuators, B*, 2014, **195**, 197–205.
- C. Ye, X. Zhong, R. Yuan and Y. Chai, *Sens. Actuators, B*, 2014, **199**, 101–107.